Soft Matter

Accepted Manuscript

ROYAL SOCIETY OF CHEMISTRY

www.rsc.org/softmatter

Journal Name

ARTICLE TYPE

Cite this: DOI: 10.1039/xxxxxxxxxx

Received Date
Accepted Date

DOI: 10.1039/xxxxxxxxxx

www.rsc.org/journalname

Active fluidization in dense glassy systems†

Rituparno Mandal,[a†] Pranab Jyoti Bhuyan,[a†] Madan Rao,[b,c] and Chandan Dasgupta *[a]

Dense soft glasses show strong collective caging behavior at sufficiently low temperatures. Using molecular dynamics simulations of a model glass former, we show that the incorporation of activity or self-propulsion, f_0, can induce cage breaking and fluidization, resulting in a disappearance of the glassy phase beyond a critical f_0. The diffusion coefficient crosses over from being strongly to weakly temperature dependent as f_0 is increased. In addition, we demonstrate that activity induces a crossover from a fragile to a strong glass and a tendency for clustering of active particles. Our results are of direct relevance to the collective dynamics of dense active colloidal glasses and to recent experiments on tagged particle diffusion in living cells.

1 Introduction

Disordered assemblies of particles approaching the glass transition, either by lowering the temperature or by increasing the density, exhibit increasingly slow dynamics and strong caging of tagged particle movement. Recently, there has been a lot of interest in the collective behavior of dense assemblies of hard-sphere-like active or self-propelled particles close to the glass transition [1–4]. In these systems, the glass transition is approached on increasing the packing fraction and the introduction of activity tends to fluidize the assembly by shifting the glass transition to higher packing fractions. The corresponding behavior in thermally controlled systems in which the glass transition occurs upon decreasing the temperature at constant density has not been explored till now.

Recent experimental studies of tagged particle diffusion in living cells make this question most pertinent. For instance, studies on tagged particle diffusion of cytoplasmic constituents[5] reveal that bacterial cytoplasm exhibits characteristic glassy features such as caging, non-ergodicity and dynamical heterogeneity in the absence of metabolic activity, and shows liquid-like features when subjected to activity through cellular metabolism. Likewise, microrheology studies of particles embedded in the cell nucleus show cage-hopping dynamics driven by active stress fluctuations arising from ATP-dependent chromatin remodeling proteins (CRPs) and complete caging in ATP-depleted conditions (or when the activity of CRPs is perturbed)[6]. Recent microrheology work on probe particles attached to cytoskeleton-motor complexes shows the effects of non-thermal fluctuations in transporting particles over large scales[7,8]. Such activity driven fluidization could play a significant role in transporting molecules over large scales, thereby regulating a variety of biochemical signaling reactions within the cell[9]. Signatures of glassy behavior have also been observed in collective cell migration[10,11], embryonic tissues [12] and active transport on disordered landscapes[13]. The importance of understanding the effects of activity on the collective dynamics of particle systems has motivated several experimental investigations involving biological[14,15] or artificially constructed[16–19] self-propelled objects.

We have studied the effects of activity on the dynamics of a thermally controlled glass-forming liquid - the Kob-Andersen binary mixture[20] - using molecular dynamics (MD) simulations. Activity is introduced in the model by assuming that a fraction ρ_a of one kind of particles in the binary system experiences a random active force f_0 that is correlated over a persistence time τ_p. In contrast to models[21,22] in which the constituent objects have fixed directions of self-propulsion, the directions of active forces in our model are not determined by the orientations of the active particles.

Our MD simulations in three dimensions were carried out using a modified leap-frog integration scheme[23]. This scheme uses

[a] Centre for Condensed Matter Theory, Department of Physics, Indian Institute of Science, Bangalore 560012, India; E-mail: cdgupta@physics.iisc.ernet.in
[b] Raman Research Institute, Bangalore 560080, India
[c] National Centre for Biological Sciences (TIFR), Bangalore 560065, India
† These authors contributed equally to this work.

velocity rescaling to simulate the behavior of systems of particles in the canonical (NVT) ensemble. The validity of this scheme has been demonstrated in many simulations (see, for example, Ref.[24]) of equilibrium glass-forming liquids. The temperature T is not well-defined in systems with activity [25,26]. In simulations of such systems, the temperature-like parameter T in the integration scheme provides an approximate measure of the average kinetic energy of the particles[27]. The dynamics generated by this integration scheme is analogous to overdamped Langevin dynamics[28,29] with the parameter T playing the role of the temperature associated with the noise in the Langevin equation. We shall refer to the parameter T as the temperature in the rest of the paper, although it may not be possible to define a temperature in an unique way in systems with activity.

There are several important differences between this model and the hard-sphere models of active glass considered in earlier studies[1–4] which make our model more suitable for describing biological systems with activity and more amenable to experimental realization. First, Lennard-Jones interactions are more faithful representations of the soft interparticle interactions in soft cytoplasmic or nuclear matter[30]. Models of active particles with soft interparticle interactions have been considered in several existing studies[21,22,28,29,31,32]. However, the dense phase in some of these studies[28,29] is (poly)crystalline because a monodisperse system of particles was considered. In contract, we consider a binary mixture that is a well-known glass-former, thereby avoiding the possibility of crystallization. Also, existing studies[21,31] in which polydispersity was used to avoid crystallization consider the liquid to glass transition as a function of the packing fraction, whereas we are interested in glass formation at fixed density as a temperature-like parameter that represents the effects of a heat bath is varied. This parameter would be easier to control in experiments than the density[5,6]. Another important difference between our model and those studied earlier is that the fraction of particles with activity is tunable in our model, whereas all the particles are assumed to be active in the models considered earlier[1–4]. This makes our model more relevant for describing biological systems such as bacterial cytoplasm[5] or nuclear matter[6] in which the fraction of active constituents can be regulated. Also, our model allows us to study separately the effects of changing the strength (f_0) and the persistence time (τ_p) of the active force. This is not possible for models[1,33] in which all the constituent particles are active and the persistence time is the only adjustable parameter because in these models, changing the correlation time of the random active force affects both the strength and the persistence time of the active force. As discussed later, these differences have important consequences for the dynamics of the system.

Our main results are : (i) Activity tends to fluidize the glass and dramatically reduces the glass transition temperature; (ii) Tagged particle dynamics shows cage-hopping resulting in a late-time diffusion coefficient that is weakly dependent on the temperature in the limit of large activity; (iii) The phase diagram in the $T - f_0$ plane shows the complete disappearance of the glass phase beyond a threshold value of the activity; (iv) The presence of activity decreases the kinetic fragility of the liquid; and (v) Activity leads to local clustering of the self-propelled particles induced by the passive particles in the glassy medium.

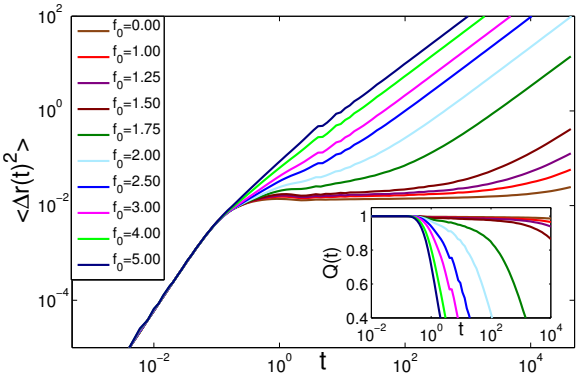

Fig. 1 MSD for the active Kob-Andersen model for different values of the self-propulsion force f_0 for $T = 0.2$, $\rho_a = 1.0$ and $\tau_p = 4.0$. Increasing activity induces cage escape and a crossover to late time diffusive behavior. Inset: Plots of the overlap function $Q(t)$ for different self-propulsion forces f_0 show a similar behavior.

2 Model

We study the Kob-Andersen binary mixture[20] with 80% A-type and 20% B-type particles interacting via the Lennard-Jones pair potential,

$$V_{ij}(r) = 4\varepsilon_{ij}\left[\left(\frac{\sigma_{ij}}{r}\right)^{12} - \left(\frac{\sigma_{ij}}{r}\right)^{6}\right], \qquad (1)$$

where r is the distance between two particles and the indices i, j can be A or B. The values of σ_{ij} and ε_{ij} are chosen to be: $\sigma_{AB} = 0.8\sigma_{AA}$, $\sigma_{BB} = 0.88\sigma_{AA}$, $\varepsilon_{AB} = 1.5\varepsilon_{AA}$, $\varepsilon_{BB} = 0.5\varepsilon_{AA}$. We set a cutoff in the potential at $r_{ij} = 2.5\sigma_{ij}$ and shift it accordingly. We set the unit of length and energy by $\sigma_{AA} = 1$, $\varepsilon_{AA} = 1$ and fix the overall density ρ at 1.2.

We introduce activity only through a fraction ρ_a of B-type particles $(0 \le \rho_a \le 1)$, while all A-type particles and a fraction $(1-\rho_a)$ of B-type particles remain passive. Thus, the number of active particles is $0.2N\rho_a$ where N is the total number of particles. The active B-particles are randomly assigned self-propulsion forces of the form $\mathbf{f_0} = f_0(k_x\hat{\mathbf{x}} + k_y\hat{\mathbf{y}} + k_z\hat{\mathbf{z}})$, where k_x, k_y, k_z are ± 1, chosen so that the net momentum of the system remains conserved. After a persistence time τ_p the directions of $\{\mathbf{f_0}\}$ are randomized by choosing a different set of k_x, k_y, k_z, while respecting momentum conservation. This discrete 8-state clock realization of the random forces shows the same qualitative features as a continuous O(3) description and all the results reported here are obtained with

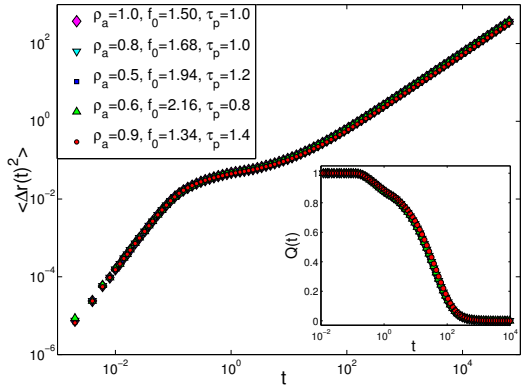

Fig. 2 MSD as a function of time at $T = 0.5$ for five different sets of values of the parameters f_0, τ_p, ρ_a, chosen such that $\zeta = \rho_a {f_0}^2 \tau_p$ remains constant at 2.25. The plots for different sets of parameter values collapse into a single curve. In the inset the collapse of the two-point correlation function $Q(t)$ for the same sets of parameter values is shown.

this scheme. Our simulations have been performed for a system with $N = 1000$ particles (800 A-type and 200 B-type particles). We have checked from simulations for $N = 5000$ at a few points in the $(f_0 - T)$ plane that finite-size effects for the quantities of interest in our study are negligible for $N = 1000$.

The details of the integration scheme used in our work are provided in Appendix A.1 where we also present representative results for the dependence of the average kinetic energies of the A and B-type particles on T for different values of f_0.

3 Numerical Results

3.1 Fluidization

To study the dynamics of the system, we measure the mean-square-displacement (MSD) of tagged particles, $\langle |\Delta \mathbf{r}(t)|^2 \rangle$, as a function of time t at different temperatures. Simultaneously, we record the two-point correlation function, $Q(t)$, whose decay in time provides a measure of the dynamical slowing down in glassy systems,

$$Q(t) = \frac{1}{N} \sum_i \langle w(|\, \mathbf{r}_i(t_0) - \mathbf{r}_i(t+t_0)\,|) \rangle \tag{2}$$

where,

$$w(r) = \begin{cases} 1 & \text{if } r \le a \\ 0 & \text{otherwise} \end{cases} \tag{3}$$

and $\langle \cdots \rangle$ represents an average over the time origin t_0. Here, N is the number of particles and the parameter a is associated with the typical amplitude of vibrational motion of the particles. For all of our analysis we have used $a = 0.3$.

At high enough temperatures, $T = 2.0$ for example, the MSD in the absence of activity ($f_0 = 0$) increases ballistically ($\sim t^2$) at short time scales, before crossing over to a diffusive ($\sim t$) regime at late times. The associated $Q(t)$ decays exponentially to zero, characteristic of a liquid. On decreasing the temperature, the MSD begins to show a small plateau at intermediate times which grows as the temperature decreases further. Simultaneously, $Q(t)$ starts exhibiting multi-step relaxation, described by a stretched exponential function at long times. At very low temperatures, e.g. for $T = 0.2$, both the MSD and $Q(t)$ remain in the plateau region over the time scales of the simulation and do not show the late time diffusive part, indicating that the system has entered a glassy state. The self-diffusion constant D, calculated from the long-time data for the MSD using the relation $\lim_{t\to\infty} \langle |\Delta \mathbf{r}(t)|^2 \rangle = 6Dt$, shows that in the absence of activity, the diffusion constant decreases very rapidly as the temperature is decreased below ~ 0.5.

Introducing activity via self-propulsion leads to a dramatic change in the dynamical behavior of the system. The behavior of the MSD and $Q(t)$, as illustrated in Fig. 1, clearly shows that the system fluidizes as the activity is increased. Detailed examination of individual trajectories of both active and passive particles shows evidence for caging at short time scales and cage breaking at longer times for relatively small values of f_0. The frequency of cage breaking increases with increasing f_0. For large f_0, caging is not present and the MSD shows a crossover from ballistic to diffusive behavior without any sign of an intermediate plateau. At high enough activity, the diffusion constant shows a large enhancement and appears to be only weakly dependent on the temperature (see Fig. 3). While the active forces in our model are characterized by 3 independent parameters, f_0, τ_p and ρ_a, we find that the combination $\zeta \equiv \rho_a {f_0}^2 \tau_p$ appears to control the dynamical behavior in the fluidized phase for variations of the individual parameters over a limited range (by factors of ~ 2). When plotted for a fixed value of ζ with different choices of f_0, τ_p, ρ_a, many dynamical quantities show a collapse, as shown in Fig. 2. The combination ζ appears naturally in a heuristic calculation of the effects of activity, based on a simple Langevin model discussed in Appendix A.2.

The time autocorrelation function of the active force on particle i in our system is given by

$$\langle f_{i\alpha}(t) f_{i\beta}(t') \rangle = \frac{1}{3} \delta_{\alpha\beta} f_0^2 (1 - |t - t'|/\tau_p) \tag{4}$$

for $|t - t'| \le \tau_p$ and zero otherwise, where α, β are coordinate labels. Approximating the dependence on $|t - t'|$ by a δ-function and considering the active force to be an additional noise term in a Langevin description, we can associate an "active temperature"[31,33,34], $(f_0^2 \tau_p)/(6\gamma k_B)$, with the active force. Here, γ is the friction coefficient appearing in the Langevin description. Taking account of the fact that only a fraction, $0.2\rho_a$, of the particles in our system are active, the effective active temperature is given by

$$T_a = \frac{C \rho_a f_0^2 \tau_p}{\gamma k_B}, \tag{5}$$

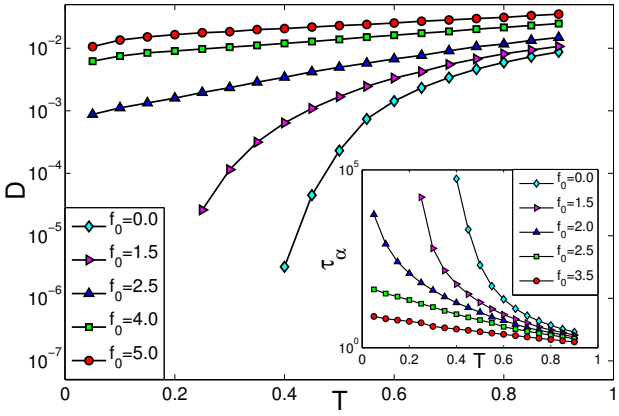

Fig. 3 The diffusion constant (D) has been plotted as a function of temperature (T) for different values of f_0 for $\tau_P = 4.0$ and $\rho_a = 1.0$. The plot shows that the dependence of the diffusion constant on the temperature becomes weaker with increasing f_0. The inset shows the α-relaxation time as a function of temperature (T) for different f_0, illustrating a qualitative change in the behavior with increasing f_0 and a reduction in the (putative) glass transition temperature.

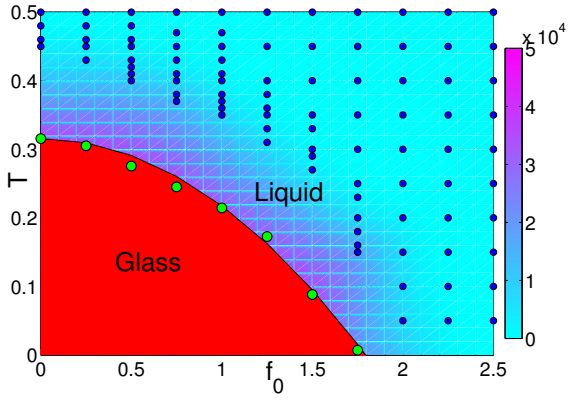

Fig. 4 Phase diagram in the $T - f_0$ plane. The blue dots indicate the points at which simulations were performed. The glass transition temperatures (green filled circles) have been obtained by fitting the α-relaxation time τ_α to extract T_{VFT} for different values of f_0. Both dimensional considerations and heuristic arguments based on a Langevin model as in Appendix A.2 suggest that the phase boundary has the form $T_{\mathrm{VFT}}(f_0) = T_{\mathrm{VFT}}(0) - A\,\rho_a \tau_p {f_0}^2$, where A is a constant of order one. The phase boundary (thin black line) represents a fit of the data for $T_{\mathrm{VFT}}(f_0)$ to this form.

where the numerical factors have been included in the constant C. As discussed below, the active temperature, which is proportional to the quantity ζ defined above, plays an important role in the activity-induced reduction of the glass transition temperature.

3.2 Structural Changes

To check whether this activity induced fluidization is accompanied by a significant change in the structure of the liquid, we have calculated the radial distribution functions $g_{\alpha\beta}(r)$, defined by

$$g_{\alpha\beta}(r) = \frac{V}{N_\alpha N_\beta} \langle \sum_{i=1}^{N_\alpha} \sum_{j=1}^{N_\beta} \delta(\mathbf{r} - \mathbf{r}_i^\alpha + \mathbf{r}_j^\beta) \rangle, \qquad (6)$$

where N_α is the number of particles of type α ($\alpha = A$ or B). We find that $g_{BB}(r)$ is more significantly affected by activity than $g_{AA}(r)$ and $g_{AB}(r)$ (Fig. 5 and Fig. 10 in Appendix A.3), and shows more liquid-like features as f_0 is increased. Also, the height of the first peak of g_{BB} decreases and a new peak at a smaller value of r develops with increasing f_0. This observation suggests that there is an activity-induced clustering tendency in the B-type particles.

The clustering tendency is confirmed from a calculation (see Appendix A.4) of the size distribution of the clusters formed by B-type particles. However, the average cluster size increases by a small amount ($< 20\%$ for the parameter values considered in our study) as the strength of the activity is increased and we do not find any evidence for activity-induced phase separation observed in many recent studies[18,19,22,28,29,31,32] of systems of active particles. Since only B-type particles are active in our model system, separation of the active component into dense and gas-like phases would also imply A-B phase separation – aggregation of a large fraction of B-type particles is necessary for the formation of a dense cluster of these particles. To check whether this happens in our system, we have divided the simulation box into a large number of cells and calculated the distribution of the number of B-type particles in each cell. These distributions for different choices of the cell size are found to be very similar to those expected for a random dispersion of the particles, indicating the absence of any large cluster of B-type particles.

One of the reasons for the absence of active phase separation in our system is that the interactions in the Kob-Andersen model are chosen specifically to avoid A-B phase separation which may lead to crystallization at high density and/or low temperature. Also, the Péclet number, defined as d_0/σ_{AA} where d_0 is the typical distance traversed by an isolated active particle in time τ_p, the time scale over which the direction of the active force remains correlated, is relatively small (< 10) for the parameter values considered in our simulation. Active phase separation is not expected[28] for such small values of the Péclet number. The choice of the Kob-Andersen model for our study also avoids the possibility of the kind of phase separation observed in Ref.[35] and the formation of microcrystalline domains.

3.3 Phase diagram

The strong effect of activity on the dynamics is seen very clearly in Fig. 3 where the temperature dependence of the long-time diffusion coefficient D has been shown for different values of the

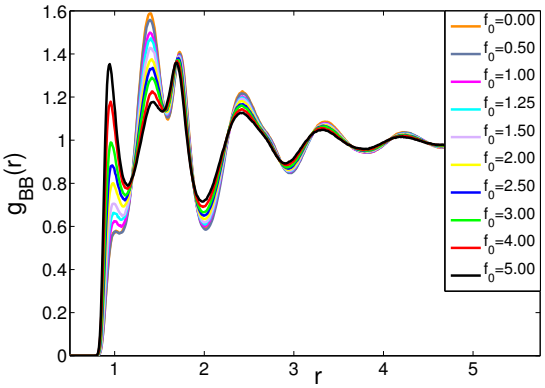

Fig. 5 Pair correlation function $g_{BB}(r)$ of B-type (active) particles for different values of f_0 at $T = 0.45$, $\rho_a = 1.0$ and $\tau_p = 4.0$. The appearance of a peak at a lower value of r and the increase in its height with the increase of activity f_0 is indicative of activity-induced clustering.

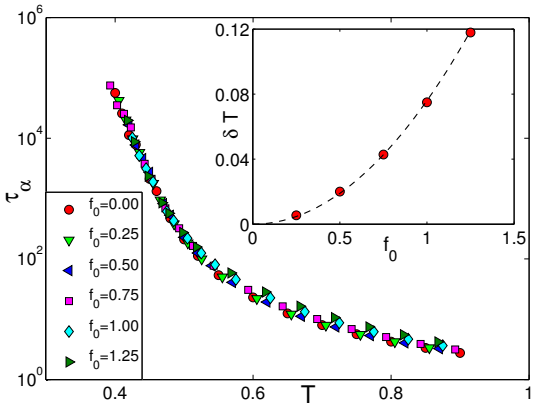

Fig. 6 Temperature dependence of the α-relaxation time for $\rho_a = 1.0$, $\tau_p = 4.0$ and different values of f_0. The temperature has been shifted by the optimal amount, $\delta T(f_0)$ (see text) for each non-zero value of f_0. Inset: Dependence of δT on f_0. The line through the data points is the best fit to a quadratic dependence.

self-propulsion force f_0. The rapid decrease in D with decreasing T for $f_0 = 0$ is replaced by a much weaker temperature dependence for large f_0. Activity-induced fluidization is also seen in plots of the α-relaxation time τ_α, extracted from the decay of $Q(t)$ ($Q(\tau_\alpha) = 1/e$), vs. T for different f_0 (inset of Fig. 3). To extract a glass transition temperature from the data for the α-relaxation time, we fit τ_α to the well-known Vogel-Fulcher-Tammann (VFT) form,

$$\tau_\alpha = \tau_\infty \exp\left[\frac{1}{\kappa\left(\frac{T}{T_{\rm VFT}} - 1\right)}\right] \qquad (7)$$

where κ is the kinetic fragility, τ_∞ is the relaxation time at high temperatures, and $T_{\rm VFT}(f_0)$ is the activity dependent (putative) glass transition temperature at which the relaxation time extrapolates to infinity.

In the absence of activity, $T_{\rm VFT}(0) \sim 0.3$ in reduced Lennard-Jones units. The values of $T_{\rm VFT}$ for different values of f_0 allow us to construct a phase diagram in the $T - f_0$ plane (Fig. 4). This shows that even at low temperatures, there is a threshold activity beyond which one may exit the glassy phase into the liquid. The magnitude of τ_α, displayed as a color plot in Fig. 4, shows a sharp increase near the phase boundary. The region displayed in red color in Fig. 4 represents infinite τ_α according to the VFT form. In this phase diagram, the glass transition temperature, defined as the temperature at which τ_α would diverge if the VFT form continues to describe its temperature dependence, approaches zero for a *finite* value (~ 1.8) of the active force f_0.

The phase boundary shown in Fig. 4 intersects the $T = 0$ axis near $f_0 = 1.8$ because the $T_{\rm VFT}$ obtained from VFT fits to the temperature dependence of τ_α at the relatively high temperatures indicated in the Figure becomes negative for larger values of f_0, suggesting that τ_α would remain finite even at $T = 0$ for such values of f_0. There are, however, indications that the extrapolation of the high-temperature results for τ_α and the diffusion coefficient D all the way down to $T = 0$ using the VFT form may not be correct for values of f_0 close to or greater than 2. As shown in Fig. 3, the temperature dependence of D for $f_0 \geq 2.5$ appears to deviate from the high-temperature behavior near $T = 0.05$, the lowest temperature at which we were able to simulate the dynamics long enough to observe clear diffusive behavior for these values of f_0. Exploratory simulations at lower temperatures suggest that the D *vs* T plot would bend downwards as T is decreased below 0.05. This would imply that the results obtained from extrapolation of the high-temperature data may not be reliable for these values of f_0. In particular, the phase boundary of Fig. 4 may not be correct near $T = 0$. To check whether there is a threshold value of f_0 above which the system is in a fluid state at $T = 0$, we have carried out simulations for large values of f_0 ($f_0 \geq 25$) at $T = 0$. We find clear evidence for diffusive behavior in these simulations. This observation clearly establishes that our model exhibits activity-induced fluidization occurring at a finite value of f_0 even at $T = 0$. However, the value of f_0 at which fluidization occurs at $T = 0$ may be higher than that shown in Fig. 4.

The occurrence of fluidization at $T = 0$ for a finite value f_0 is not surprising because, as mentioned earlier, the dynamics used in our simulation reduces to overdamped Langevin dynamics with zero noise in the $T \to 0$ limit. The average kinetic energy of the particles is not zero in this limit because of the presence of the active force. This is sufficient to melt the glass if f_0 is sufficiently large.

As discussed in detail in Appendix A.2, a heuristic single-particle Langevin model provides a rationalization of some of the features observed in our simulations. In this model, the phase

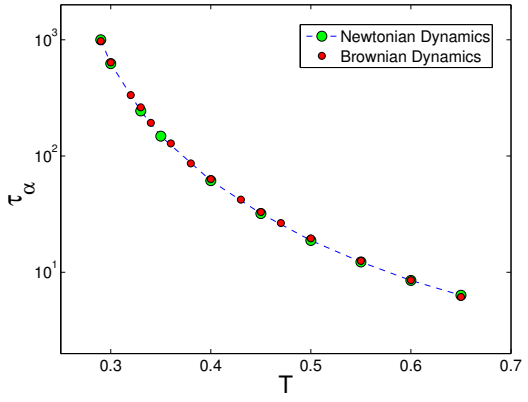

Fig. 7 Relaxation time (τ_α) as a function of temperature T, obtained from Newtonian MD and overdamped Langevin (Brownian) dynamics simulations.

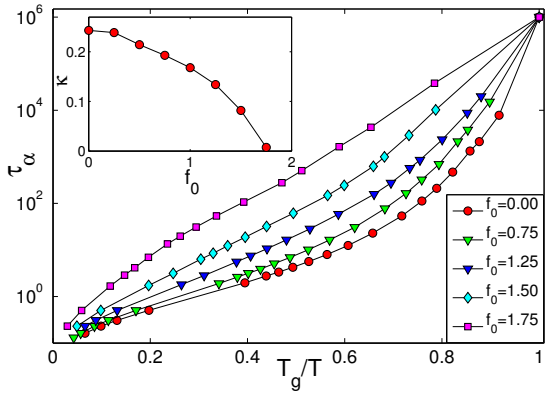

Fig. 8 Angell plot showing a crossover from fragile to strong behavior with increasing active force (f_0). In the inset, the kinetic fragility (κ) has been plotted as a function of f_0.

boundary in the $(f_0 - T)$ plane has the form

$$T_{\rm VFT}(f_0) = T_{\rm VFT}(0) - A\rho_a\tau_p {f_0}^2, \qquad (8)$$

where A is a constant of order unity. As shown in Fig. 4, this form provides a good description of the simulation results for small values of f_0. This observation indicates that the shift in the glass transition temperature due to the presence of activity is proportional to the "active temperature" T_a defined in Eq. 5 which is proportional to the quantity $\zeta \equiv \rho_a {f_0}^2 \tau_p$ in our system. This is in agreement with the results of mode-coupling calculations[33,36] which predict that the effect of activity in systems where the activity is a relatively small perturbation to the thermal behavior is similar to that of increasing the temperature in the system without activity.

As a further check of the validity of this description, we have tried to collapse the data for the α-relaxation time shown in the inset of Fig. 3 into a single master curve by shifting the temperature by an amount that depends on the value of f_0. For each nonzero value of f_0, we find the temperature shift $\delta T(f_0)$ that minimizes the difference between the curves $\tau_\alpha(T - \delta T, f_0)$ and $\tau_\alpha(T, f_0 = 0)$. Results of this analysis are shown in Fig. 6 where the data for each nonzero value of f_0 have been plotted with the optimal temperature shift $\delta T(f_0)$. With this shift, the curves for different values of f_0 show fairly good collapse, although there are small systematic differences between the curves. In the inset of Fig. 6, we have shown the dependence of δT on f_0. It is clear that δT is proportional to f_0^2, as expected from Eq. 5. Using the best-fit value of the constant of proportionality and Eq. 5, we estimate the value of the friction coefficient γ in the equivalent Langevin description to be close to 1.8. We have carried out a test simulation for $f_0 = 1.5$ using overdamped Langevin dynamics with $\gamma = 1.8$. The temperature dependence of τ_α found in this simulation is very similar to that obtained in our MD simulation. Fig. 7 shows the temperature dependence of the relaxation time τ_α obtained from these two approaches. To show the correspondence between the two sets of results clearly, the τ_α values obtained from overdamped Langevin dynamics has been scaled by a factor of 2.0. These results establish a correspondence between our MD simulations and overdamped Langevin dynamics and support the conclusion that the effect of activity on the dynamics of our system can be described as that of increasing the temperature by T_a.

Figure 8 shows so-called "Angell Plots" - τ_α vs T_g/T, where T_g, the analog of the experimentally determined glass transition temperature at which the viscosity is 10^{13} poise, is obtained from the definition $\tau_\alpha(T_g) = 10^6$. The curvature of the plots decreases with increasing f_0, indicating that the fragility decreases with increasing activity. The dependence of the kinetic fragility κ obtained from the VFT fits on the active force f_0 (see the inset of Fig. 8) exhibits the same trend, indicating that the activity makes the glass stronger.

4 Discussion and Conclusions

There are several observable features of our model that are qualitatively different from those found in earlier studies[1,2] of activity-driven fluidization. In our model, the glass transition disappears beyond a "critical" value of the activity, whereas in Refs.[1] and[2], the glass transition was found to be present for all finite values of the strength of the activity. This reflects a fundamental difference between hard-sphere systems and those with soft interactions. In our model, the diffusion constant increases as f_0 is increased from zero at all temperatures. This behavior is qualitatively different from that reported in Ref.[1] where the diffusion constant was found to *decrease* with increasing activity at relatively low densities (equivalent to relatively high temperatures

in our system), causing a crossing of D vs. ρ plots for different strengths of the activity. In our system (also in Ref.[2]), D vs. T plots for different f_0 come closer to each other as T is increased, but they do not cross. This difference is probably a consequence of the fact that the only control parameter considered in Ref.[1] is the correlation time of the random force which, as discussed earlier, affects both the strength and the persistence time of the active forces. Contrary to the behavior of the hard-sphere system studied in Ref.[2], we find that the fragility in our model system decreases with increasing activity.

These observations tell us that some of the effects of activity on the glass transition are sensitive to the nature of the system (whether driven by temperature or density) and to the details of the self-propulsion mechanism[37]. This would imply that some of the detailed characteristics of the active forces present in an experimentally studied system must be included in the development of models for explaining the observed behavior.

To summarize, we have demonstrated activity driven fluidization in a model glass former at low temperatures and a concomitant reduction of the glass transition temperature with increasing activity. This fluidization is accompanied by a crossover from caging dynamics to diffusive transport at long times. The late-time diffusion coefficient in the activity-induced fluid phase is weakly dependent on the temperature. We display a phase diagram in the $T - f_0$ plane that suggests that the glass transition temperature goes to zero at a finite threshold value of f_0. The shape of the phase boundary has been rationalized from a simple calculation as in Appendix A.2. This calculation also brings forth the possibility of existence of a single control parameter, $\zeta = \rho_a {f_0}^2 \tau_p$, constructed from the three parameters ρ_a, f_0 and τ_p that characterizes the effects of activity on the dynamics of the system in the fluid phase. This quantity plays the role of an "active temperature" that adds to the nominal kinetic temperature of the thermal system. We have also observed an activity induced clustering of the self-propelled particles. The kinetic fragility of the glass former has been found to decrease with increase in activity. The results obtained here should be relevant to activity induced fluidization in a variety of dense colloidal systems and in cells and tissues. We are currently exploring variants of this model to explain specific features of caging and fluidization observed in the cell surface and the nucleus.

A Appendix

A.1 Integration scheme

An elementary time step of the integration scheme used in our study (Ref.[23]) involves the following operations:

$$\vec{v}_i'(t) = \vec{v}_i(t - \Delta t/2) + \vec{F}_i(t)\Delta t/2m, \tag{9}$$

$$\beta^2 = \frac{(3(N-1)k_B T/m)}{\sum_{i=1}^{N} |\vec{v}_i'(t)|^2}, \tag{10}$$

$$\vec{v}_i(t + \Delta t/2) = \vec{v}_i(t - \Delta t/2)(2\beta - 1) + \beta \vec{F}_i(t)\Delta t/m. \tag{11}$$

Here, Δt is the integration time step, $\vec{v}_i(t)$ is the velocity of particle i at time t, m is the mass of a particle, and $\vec{F}_i(t)$ is the force on particle i arising from its interaction with the other particles. For the active particles, we add the contribution from the active force $f_0 \hat{n}_i(t)$:

$$\vec{v}_i(t + \Delta t/2) = \vec{v}_i(t + \Delta t/2) + f_0 \hat{n}_i(t)\Delta t/m \tag{12}$$

where, $\hat{n}_i(t)$ is the direction of the active force on particle i. This vector changes after a persistence time τ_p. The positions of the particles are then updated and the forces are calculated:

$$\vec{r}_i(t + \Delta t) = \vec{r}_i(t) + \vec{v}_i(t + \Delta t/2)\Delta t \tag{13}$$

$$\vec{F}_i(t + \Delta t) = -\sum_{j=1}^{N} \vec{\nabla}_i \Phi(\vec{r}_i(t + \Delta t), \vec{r}_j(t + \Delta t)) \tag{14}$$

where the sum over j excludes the $j = i$ term, $\vec{\nabla}_i$ represents the derivative with respect to $\vec{r}_i$ and Φ is the pair interaction potential.

The results reported in the paper were obtained using this integration scheme in which the velocities are rescaled in every time step. We have also carried out simulations in which velocity rescaling is performed at intervals of n time steps with $1 < n \leq 10$, and found that the results are insensitive to the value of n in this range.

To examine how the average kinetic energies of the active and passive particles depend on T, we have shown in Table.1 the values of the average kinetic energy (per particle) of both active and passive particles for several representative values of T and f_0. These results were obtained from simulations with 2.5×10^6 time steps with $\Delta t = 0.002$. Averages were performed over 100 data points at equal intervals. The error bars (numerical uncertainty in determining the average from a finite number of measurements) were estimated from the standard deviation of the 100 data points. It can be seen from the numbers in this Table that the average kinetic energy of the passive particles is very close to the equipartition value, $3k_B T/2$. The deviations from the equipartition value are less than 0.5%, comparable to the error bars and the deviations found in simulations in the absence of ac-

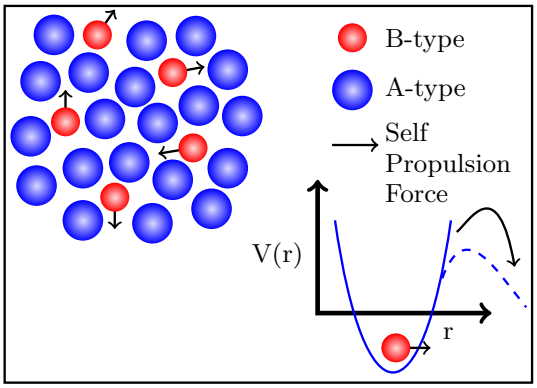

Fig. 9 Schematic diagram (in the top left) for self-propelled dynamics and (in the right bottom) for the effective dynamics of B-type particles in the presence of activity in a cage-like environment, represented by a caging potential V. Activity generates an athermal noise for B-type particles and remodels the caging-potential to allow for escape.

tivity ($f_0 = 0$). The average kinetic energy of the active particles is higher than that of the passive particles by 1-2%, depending on the values of T and f_0. Thus, the kinetic energy per particle, averaged over both active and passive particles, is slightly higher than that for the passive particles which, in turn, is very close to $3k_BT/2$.

A.2 Heuristic Calculation

As described in the main text, a dense soft glass-forming liquid, modeled by the Kob-Andersen binary mixture of A-type and B-type particles, shows strong collective caging behavior at sufficiently low temperatures. Incorporating activity or self-propulsion, f_0, in B-type particles induces cage breaking and fluidization if f_0 is sufficiently large. Here we try and capture some features of this collective behavior within an approximate single-particle description, using Langevin dynamics for the position of a tagged-particle in an effective caging potential created by the neighboring particles. Activity enters into the Langevin equation both as a source of athermal noise[14] and as a slower remodeling of the caging potential (Fig. 9).

We model the dynamics of a tagged passive particle by a Langevin equation for the displacement $x_A(t)$,

$$m\ddot{x}_A = -V' - \gamma\dot{x}_A + \xi(t)\,, \tag{15}$$

where m is the mass of a particle (assumed to be the same for both active and passive particles) and γ is the effective friction coefficient. V' is the force derived from a caging potential whose form we comment on later. The thermal noise $\xi(t)$ is taken to be white having zero mean with a variance equal to $2\gamma k_BT$. As noted in the main paper, the parameter T in our simulations is analogous to the temperature associated with the noise term in the Langevin equation.

The active particles are, in addition, subject to a random active force with amplitude f_0. The randomness is modeled by an athermal noise $\psi(t)$, which is exponentially correlated over a time scale τ_p. The Langevin equation describing its displacement is given by,

$$m\ddot{x}_B = -V' - \gamma\dot{x}_B + \xi(t) + f_0\,\psi(t)\,. \tag{16}$$

The statistics of the athermal noise is given by $\langle\psi(t)\rangle = 0$, $\langle\xi(t)\psi(t')\rangle = 0$ and

$$\langle\psi(t)\psi(t')\rangle = c\exp\left[-\frac{|t-t'|}{\tau_p}\right] \tag{17}$$

where c is a dimensionless constant. For a fixed τ_p and c, this athermal noise in general does not obey the fluctuation-dissipation relation. The fraction of active particles is ρ_0 which is equal to $0.2\rho_a$ in the model considered in our simulations.

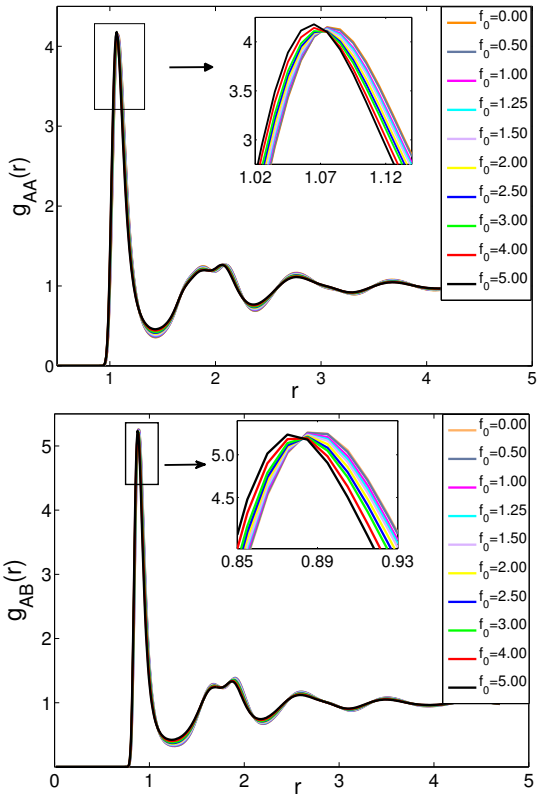

Fig. 10 Changes in pair correlation function (a) (top) $g_{AA}(r)$ and (b) (bottom) $g_{AB}(r)$ in the presence of different values of self-propulsion forces (f_0) for $T = 0.45$, $\rho_a = 1.0$ and $\tau_P = 4.0$. Insets in the figures show the shift of the first peak of $g(r)$ to lower values of r with increasing f_0, suggesting formation of structures at smaller scales.

The caging potential V (Fig. 9) is taken to have the same form for both active and passive particles, with a confining harmonic

part, $V = \frac{1}{2}kx_\alpha^2$ (where $\alpha = A,B$), and a barrier whose height is reduced by the active force over a time scale corresponding to the α-relaxation time. In what follows, we will only be concerned with the harmonic confining part of the potential, represented by the parameter k.

It is straightforward to calculate the mean square displacement of the active and passive particles,

$$\langle [x_A(t)]^2 \rangle = \frac{k_B T}{k} \tag{18}$$

$$\langle [x_B(t)]^2 \rangle = \frac{k_B T}{k} + \frac{f_0^2 c \tau_p}{\gamma k} \frac{1}{(1+\frac{\tau_p}{\tau_x})}, \tag{19}$$

where the relaxation time $\tau_x = \gamma/k$. The particle-averaged mean square displacement may be written as,

$$\langle x(t)^2 \rangle = \rho_0 \langle x_B(t)^2 \rangle + (1-\rho_0)\langle x_A(t)^2 \rangle, \tag{20}$$

from which we can derive an average Lindemann factor,

$$\frac{\langle x^2 \rangle}{a^2} = \frac{k_B T}{ka^2} + \frac{\rho_a {f_0}^2 \tau_p}{\gamma k a^2} \left[\frac{c}{1+\frac{\tau_p}{\tau_x}} \right] \tag{21}$$

Here, a is the typical cage size, ka^2 is the potential energy scale, and the ratio ρ_0/ρ_a has been absorbed by redefining the constant c. The coefficient of the second term on the right-hand side of Eq. 21 is proportional to $k_B T_a/(ka^2)$ for $\tau_p \ll \tau_x$ where T_a is the "active temperature" defined in Eq. 5. This equation implies that the effect of activity in this system can be approximated as that of increasing the bath temperature by an amount proportional to T_a. This gives us a heuristic phase boundary which varies with the self-propulsion force as $T_{\rm VFT}(f_0) = T_{\rm VFT}(0) - A\rho_a \tau_p {f_0}^2$ where A is a proportionality constant. As discussed in the main paper, this form provides a good description of the phase boundary found in our simulations. The form of Eq. 21 is also consistent with the observation that different combinations of the parameters ρ_a, f_0 and τ_p for a constant value of $\zeta = \rho_a {f_0}^2 \tau_p$ lead to a collapse of dynamical quantities such as the MSD and $Q(t)$ in a temperature range above the VFT temperature, $T_{\rm VFT}$.

A.3 Pair Correlation Functions

The pair correlation function $g_{\alpha\beta}(r)$ is defined as

$$g_{\alpha\beta}(r) = \frac{V}{N_\alpha N_\beta} \langle \sum_{i=1}^{N_\alpha} \sum_{j=1}^{N_\beta} \delta(\mathbf{r} - \mathbf{r}_i^\alpha + \mathbf{r}_j^\beta) \rangle, \tag{22}$$

where N_α is the number of particles of type α ($\alpha = A$ or B).

As shown in Fig. 10, $g_{AA}(r)$ and $g_{AB}(r)$ are less affected by the presence of activity compared to $g_{BB}(r)$, which shows a significant change with increasing activity. This suggests that presence of stochastic activity does not affect the local structure of the passive A-type particles in any significant manner, whereas the B-type particles are affected much more strongly. This observation also rules out the occurrence of A-B phase separation and the formation of crystallites in the presence of activity.

A.4 Evidence of activity induced clustering

To understand the decrease of the first peak height and the simultaneous development of a new peak at a smaller value of r in $g_{BB}(r)$, we analyze the cluster size distribution for the B-type particles. For this purpose, we define two B-particles to be connected if their interparticle distance is less than a cutoff r_0, chosen to be slightly larger than the value of r at the new peak in $g_{BB}(r)$ that appears with increasing activity (we have taken r_0=1.0 for the results shown in Fig. 11).

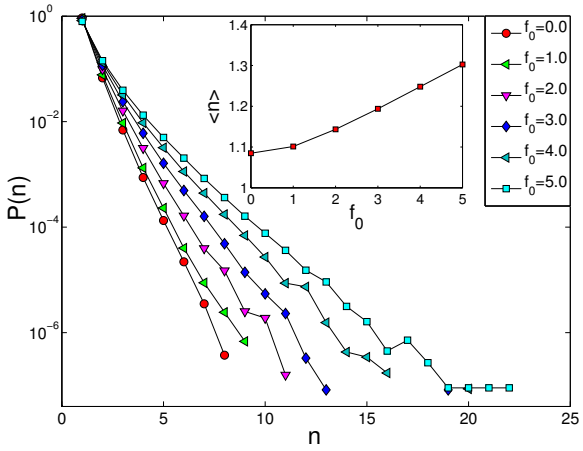

Fig. 11 Cluster size distribution function $P(n)$, where n is the size of a cluster of the B-type particles, for different f_0 at $T = 0.45$, $\rho_a = 1.0$ and $\tau_p = 4.0$. With increasing activity (f_0), the distribution broadens, signifying the clustering tendency of B-type particles. In the inset the average cluster size has been plotted as a function of f_0.

f_0	Particle Type	$T = 0.05$	$T = 0.25$	$T = 0.50$	$T = 0.75$	$T = 1.00$
0.0	Passive(A)	0.0500 $\pm$0.0001	0.2504 $\pm$0.0003	0.5008 $\pm$0.0006	0.7519 $\pm$0.0010	1.0022 $\pm$0.0013
	Passive(B)	0.0503 $\pm$0.0002	0.2510 $\pm$0.0012	0.5024 $\pm$0.0025	0.7517 $\pm$0.0039	1.0044 $\pm$0.0050
1.0	Passive(A)	0.0503 $\pm$0.0001	0.2503 $\pm$0.0003	0.5005 $\pm$0.0006	0.7486 $\pm$0.0010	0.9982 $\pm$0.0012
	Active(B)	0.0510 $\pm$0.0003	0.2537 $\pm$0.0013	0.5017 $\pm$0.0025	0.7521 $\pm$0.0038	1.0049 $\pm$0.0045
2.0	Passive(A)	0.0504 $\pm$0.0001	0.2487 $\pm$0.0003	0.4997 $\pm$0.0007	0.7500 $\pm$0.0017	0.9998 $\pm$0.0023
	Active(B)	0.0518 $\pm$0.0003	0.2502 $\pm$0.0013	0.5022 $\pm$0.0026	0.7581 $\pm$0.0041	1.0109 $\pm$0.0056

Table 1 Average kinetic energy per particle of the passive (A) and the active (B) particles for a number of parameter values (T, f_0). The simulations were performed with $\rho_a = 1.0$ and $\tau_p = 4.0$.The values of the kinetic energies are in units of $3k_B/2$.

5 Acknowledgements

We thank Saurish Chakrabarty and Akshay Bhatnagar for useful discussions. R. M. and P. J. B. acknowledges financial support from CSIR, India. C. D. acknowledges financial support from DST, India. M. R. acknowledges a grant from the Simons Centre.

Notes and references

1 L. Berthier, *Phys. Rev. Lett.*, 2014, **112**, 220602.
2 R. Ni, M. A. C. Stuart and M. Dijkstra, *Nat. Commun.*, 2013, **4**, 2704.
3 G. Szamel, E. Flenner and L. Berthier, *Phys. Rev. E*, 2015, **91**, 062304.
4 R. Ni, M. A. Cohen Stuart, M. Dijkstra and P. G. Bolhuis, *Soft Matter*, 2014, **10**, 6609–6613.
5 B. R. Parry, I. V. Surovtsev, M. T. Cabeen, C. S. OâĂŹHern, E. R. Dufresne and C. Jacobs-Wagner, *Cell*, 2014, **156**, 183 – 194.
6 F. M. Hameed, M. Rao and G. V. Shivashankar, *PLoS ONE*, 2012, **7**, e45843.
7 N. Fakhri, A. D. Wessel, C. Willms, M. Pasquali, D. R. Klopfenstein, F. C. MacKintosh and C. F. Schmidt, *Science*, 2014, **344**, 1031–1035.
8 M. Guo, A. J. Ehrlicher, M. H. Jensen, M. Renz, J. R. Moore, R. D. Goldman, J. Lippincott-Schwartz, F. C. Mackintosh and D. A. Weitz, *Cell*, 2014, **158**, 822 – 832.
9 A. Chaudhuri, B. Bhattacharya, K. Gowrishankar, S. Mayor and M. Rao, *Proceedings of the National Academy of Sciences*, 2011, **108**, 14825–14830.
10 T. E. Angelini, E. Hannezo, X. Trepat, M. Marquez, J. J. Fredberg and D. A. Weitz, *Proceedings of the National Academy of Sciences*, 2011, **108**, 4714–4719.
11 D. Bi, X. Yang, M. C. Marchetti and M. L. Manning, *arXiv:1509.06578v3*, 2015.
12 E.-M. Schötz, M. Lanio, J. A. Talbot and M. L. Manning, *Journal of The Royal Society Interface*, 2013, **10**, 0726.
13 C. Reichhardt and C. J. Olson Reichhardt, *Phys. Rev. E*, 2014, **90**, 012701.
14 C. Maggi, M. Paoluzzi, N. Pellicciotta, A. Lepore, L. Angelani and R. Di Leonardo, *Phys. Rev. Lett.*, 2014, **113**, 238303.
15 H. M. López, J. Gachelin, C. Douarche, H. Auradou and E. Clément, *Phys. Rev. Lett.*, 2015, **115**, 028301.
16 V. Narayan, S. Ramaswamy and N. Menon, *Science*, 2007, **317**, 105–108.
17 W. T. Kranz, M. Sperl and A. Zippelius, *Phys. Rev. Lett.*, 2010, **104**, 225701.
18 I. Theurkauff, C. Cottin-Bizonne, J. Palacci, C. Ybert and L. Bocquet, *Phys. Rev. Lett.*, 2012, **108**, 268303.
19 J. Palacci, S. Sacanna, A. P. Steinberg, D. J. Pine and P. M. Chaikin, *Science*, 2013, **339**, 936–940.
20 W. Kob and H. C. Andersen, *Phys. Rev. Lett.*, 1994, **73**, 1376–1379.
21 S. Henkes, Y. Fily and M. C. Marchetti, *Phys. Rev. E*, 2011, **84**, 040301.
22 B. M. Mognetti, A. Šarić, S. Angioletti-Uberti, A. Cacciuto, C. Valeriani and D. Frenkel, *Phys. Rev. Lett.*, 2013, **111**, 245702.
23 D. Brown and J. Clarke, *Molecular Physics*, 1984, **51**, 1243–1252.
24 S. Sengupta, S. Karmakar, C. Dasgupta and S. Sastry, *Phys. Rev. Lett.*, 2012, **109**,.
25 N. Kikuchi, A. Ehrlicher, D. Koch, J. A. Käs, S. Ramaswamy and M. Rao, *Proceedings of the National Academy of Sciences*, 2009, **106**, 19776–19779.
26 C. Battle, C. P. Broedersz, N. Fakhri, V. F. Geyer, J. Howard, C. F. Schmidt and F. C. MacKintosh, *Science*, 2016, **352**, 604–607.
27 In the presence of active forces, the average kinetic energy per particle of the active (B-type) particles is slightly higher than that of the passive (A-type) particles. Since the fraction of active particles is small ($\leq 20\%$) in our system, the average kinetic energy is close to that of the A-type particles which, in turn, is very close to the equipartition value, $3k_BT/2$. See Appendix A.1 for more details.
28 G. S. Redner, M. F. Hagan and A. Baskaran, *Phys. Rev. Lett.*, 2013, **110**, 055701.
29 A. Wysocki, R. G. Winkler and G. Gompper, *Europhys. Lett.*, 2014, **105**, 48004.
30 K. E. Kasza, A. C. Rowat, J. Liu, T. E. Angelini, C. P. Brangwynne, G. H. Koenderink and D. A. Weitz, *Current Opinion in Cell Biology*, 2007, **19**, 101 – 107.
31 Y. Fily, S. Henkes and M. C. Marchetti, *Soft Matter*, 2014, **10**, 2132.
32 I. Buttinoni, J. Bialke, F. Felix Kümmel, H. Löwen, C. Bechinger and T. Speck, *Phys. Rev. Lett.*, 2013, **110**, 238301.
33 G. Szamel, E. Flenner and L. Berthier, *Phys. Rev. E*, 2015, **91**, 062304.
34 T. F. F. Farage, P. Grinninger and J. M. Brader, *Phys. Rev. E*, 2015, **91**, 042310.
35 X. Yang, M. L. Manning and M. C. Marchetti, *Soft Matter*, 2014, **10**, 6477.
36 T. F. F. Farage and J. M. Brader, *arXiv:1403:0928v2*, 2014.
37 L. Berthier and J. Kurchan, *Nat. Phys.*, 2013, **9**, 310–314.